Title

Influence of Endo- and Exocyclic Heteroatoms on Stabilities and 1,3-Dipolar Cycloaddition Reactivities of Mesoionic Azomethine Ylides and Imines

Journal

The Journal of Organic Chemistry, 82(20)

ISSN

0022-3263

Authors

Champagne, Pier Alexandre
Houk, KN

Publication Date

2017-10-20

DOI

10.1021/acs.joc.7b01928

Peer reviewed

Published in final edited form as:

J Org Chem. 2017 October 20; 82(20): 10980–10988. doi:10.1021/acs.joc.7b01928.

Influence of Endo- and Exocyclic Heteroatoms on Stabilities and 1,3-Dipolar Cycloaddition Reactivities of Mesoionic Azomethine Ylides and Imines

Pier Alexandre Champagne[iD] and **K. N. Houk**[*,iD]

Department of Chemistry and Biochemistry, University of California, Los Angeles, California 90095, United States

Abstract

The geometries, stabilities, and 1,3-dipolar cycloaddition reactivities of 24 mesoionic azomethine ylides and imines were investigated using density functional theory calculations at the M06-2X/6-311+G-(d,p)/M06-2X/6-31G-(d) level. The computed structures highlight how the commonly used "aromatic" resonance form should be replaced by two more accurate resonance structures. Stabilities of the dipoles were assessed by various homodesmotic schemes and are consistent with these compounds being nonaromatic. The activation free energies with ethylene or acetylene range from 11.8 to 36.6 kcal/mol. Within each dipole type, the predicted cycloaddition reactivities correlate with the reaction energies and the resonance stabilization energies provided by the various substituents. Endocyclic (X) heteroatoms increase the reactivity of the 1,3-dipoles in the order of O > NH ≅ S, whereas exocyclic (Y) substituents increase it in the order of CH_2 > NH > O > S. Distortion/interaction analysis indicated that the difference in reactivity between differently substituted 1,3-dipoles is driven by distortion, whereas the difference between azomethine ylides and imines is related to lower interaction energies of imines with the dipolarophiles.

Graphical abstract

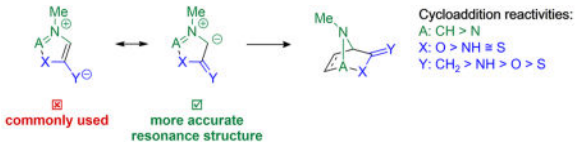

[*]**Corresponding Author**. houk@chem.ucla.edu.

ORCID

Pier Alexandre Champagne: 0000-0002-0546-7537

K. N. Houk: 0000-0002-8387-5261

ASSOCIATED CONTENT

Supporting Information

The Supporting Information is available free of charge on the ACS Publications website at DOI: 10.1021/acs.joc.7b01928.

Full computational details, complete list of authors for the Gaussian 09 reference; additional figures, tables, and discussion; Cartesian coordinates, energies, free energies, and vibrational frequencies of all structures (PDF)

The authors declare no competing financial interest.

INTRODUCTION

Mesoionic compounds are a class of five-membered heterocycles that can only be represented by zwitterionic all-octet Lewis structures.[1] There are many potential mesoionic molecules, only some of which have been synthesized. The most common type of mesoionic ring system, called type A (Figure 1A), has trivalent groups at the a and c positions, whereas b and X are divalent or trivalent heteroatoms.[2] Resonance form **III** is the traditional "mesoionic" representation for such systems, as it suggests a 6π-electron cyclic aromatic character for the species. We show below that resonance forms **I** and **II** better represent the electronic structures of the compounds. Within type A mesoionic compounds, the most common systems are called münchnones[3, 4] or sydnones,[5, 6] which contain N^+–R at the b position and O at the X and Y positions (Figure 1B). These are 1,3-dipoles, specifically azomethine ylides (AY) and azomethine imines (AI) (green atoms in Figure 1). When engaged in cycloaddition reactions with various kinds of dipolarophiles, these mesoionic compounds form a cycloadduct that quickly undergoes retro-cycloaddition with expulsion of CO_2, as exemplified for a generic münchnone in Figure 1C. For münchnones and sydnones, the first step of this process is rate-determining, and the loss of CO_2 is spontaneous, but some examples of isolable cycloadducts are known when other heteroatoms are present at the X and Y positions.[1]

Münchnones and sydnones are useful 1,3-dipoles because they are more stable than acyclic azomethine ylides and imines and generate pyrrole or pyrazole products upon cycloadditions with alkynes. These properties have been used to approach such heterocycles in total synthesis,[7] methodology development,[8] materials science,[9] and, more recently, bioorthogonal applications.[10] In our continued computational investigation of novel bioorthogonal cycloaddition partners based on 1,3-dipoles, we discovered that 3-phenyl sydnone imine **ii** is more reactive toward cyclooctyne ($\Delta G^{\ddagger}$ = 22.2 kcal/mol) than the corresponding sydnone **i** ($\Delta G^{\ddagger}$ = 24.8), while acetyl-sydnone imine **iii** is slightly less reactive ($\Delta G^{\ddagger}$ = 25.1) (Figure 2).[11]

This interesting result intrigued us about how endocyclic (X) and exocyclic (Y) substitution affects the stability and cycloaddition reactivity of mesoionic 1,3-dipoles. We now report the results of our theoretical investigations of those compounds. We chose to study the cycloaddition reactions of model azomethine ylides **1–12** and azomethine imines **13–24** with both acetylene (a) and ethylene (b) as model dipolarophiles (Table 1). Each of the possible X and Y atoms has precedents in the literature, although we could not find examples of every combination that is studied here. These reported compounds always bear additional substituents at various positions (examples in Figure 3), and most (but not all) of them were tested for their cycloaddition reactivities. Our study focused on the cycloaddition step of the mechanism because it is almost always irreversible (see below) and thus independent of the retro-cycloaddition of the X═C═Y group.[12]

COMPUTATIONAL METHODS

Density functional theory (DFT) calculations were performed using Gaussian 09.[11, 16] Geometry optimizations were carried out for the gas phase with the M06-2X functional,[17]

which was shown to provide accurate results for cycloaddition reactions,[18] using the 6-31G-(d) basis set. Normal mode vibrational analysis on the stationary points allowed us to verify if they are minima (zero imaginary frequency) or transition structures (TS, one imaginary frequency). ZPE, enthalpy, and free energy corrections were obtained using a standard state of 1 atm of pressure and 298 K. Free energies were computed using Truhlar's quasiharmonic oscillator approximation, setting all frequencies below 100 to 100 cm^{-1}.[19] To obtain accurate energies, single-point energy refinements were then performed at the M06-2X/6-311+G-(d,p) level of theory. Frontier molecular orbitals (FMOs) and their energies were computed at the HF/6-311++G-(d,p) level, using the M06-2X-optimized geometries. Computed structures were visualized using CYLview.[20]

RESULTS AND DISCUSSION

Geometries and Stabilities of Mesoionic Ring Systems

The structures and properties of mesoionic ring systems were subjects of research quickly after they were first reported. Decades of work on X-ray crystallography, semi-empirical calculations, reactivity studies, and NMR analyses of such systems were reviewed in 1998 by Simas and co-workers.[21] They concluded that type A mesoionic compounds do not fit any of the geometric, energetic, or magnetic criteria for aromaticity[22] and that the use of resonance form **III** (Figure 1) should be discontinued. We have analyzed the M06-2X/6-31G-(d) geometries of **1–24**, and the structures of münchnone **1** and sydnone **13** are shown in Figure 4 as representative examples. The structures of the other dipoles that we have studied, all of which are planar, can be found in Figures S1 and S2. While we are aware that the numbering of these heterocycles should be different when X = NR or S, we keep the numbering associated with münchnones or sydnones (X = O) for the following discussion.

In *N*-methyl münchnone **1**, the C(5)═O bond is 1.20 Å and the C(5)–O(1) bond is 1.51 Å; these have strong double- and single-bond characters, respectively. Moreover, the O(1)–C(2) bond is shorter (1.30 Å), indicative of a bond order between single and double. The C(2)–N(3) and C(4)–N(3) bonds are of different lengths (1.31 vs 1.39 Å), with the former very close to a typical C═N bond (1.29 Å). Finally, the C(4)–C(5) bond has a length of 1.40 Å, between a single and double carbon–carbon bond. The other AY **2–12** all show the same trends; double bond character at the C(5)═Y and C(2)–N(3) bonds, pure single bond at the C(5)–X position, and mixed single/double bond for the other bonds (Figure S1 and Table S2). In AI **13–24**, the trends described above are all present. In **13**, the N(2)–N(3) bond (1.29 Å) is very close to the typical N═N bond distance (1.25 Å), whereas the N(3)–C(4) bond length of 1.34 Å indicates a bond order almost exactly between a double and single C–N bond. Other AI **14–24** have similar geometrical parameters (Figure S2 and Table S3).

The variance in lengths between bonds connecting the same atom types indicates that the geometric criteria for aromaticity is not respected in mesoionic azomethine ylides or imines.[22] Our observations are in agreement with recent DFT studies of similar compounds, where bonding, charges, and magnetic analyses confirmed the absence of aromaticity.[23] Although it is known that multiple resonance forms are required to properly describe mesoionic compounds,[23b] one has to be chosen for drawing purposes. We propose that resonance structure **I**, which shows a C═Y double bond and highlights the 1,3-dipolar

nature of the ring systems, is more consistent with the actual geometries of AY and should be used. For AI, both **I** and **II** are reasonable, due to the ambiguous nature of the N(3)–C(4) bond, but we propose that **II** should be favored.

Another criterion for aromaticity is the energetic stabilization obtained from resonance delocalization.[22] Schleyer previously devised a general homodesmotic equation to assess the aromaticity of five-membered heterocycles (eq 1),[24] which was recently applied to some heterocyclic betaines.[23c, 25] When applied to the most commonly used resonance structures of AY **1–12** (e.g., **1** in eq 2), this scheme predicted that most of them are anti-aromatic (negative Δ*E*, Table S4). In addition, it predicted that the most reactive dipoles (see below) are also the most aromatic. We believe these issues are related to the fact that this scheme, as are all other homodesmotic equations, is designed for compounds that can be defined by a single Lewis structure. Mesoionic dipoles do not fit this description, and choosing a different resonance structure will inevitably yield a different result (see eq S3). Moreover, we and others have shown that

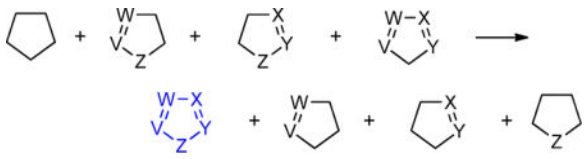

(1)

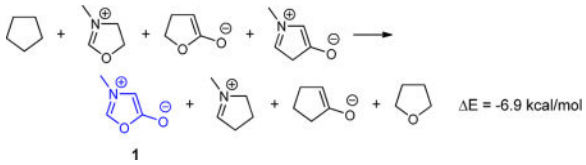

1

(2)

the resonance structure of eq 2 is not even a good representation of the geometries of mesoionic dipoles. Finally, the analysis of such compounds, which are formally neutral, requires dissecting them into *charged* reference structures, and this might be another reason for such a failure.

To solve these problems, we designed a simpler homodesmotic equation that is consistent with our proposed resonance structures and where no charged reference compounds are used (eq 3). An example, applied to AI **24**, is shown in eq 4. This equation

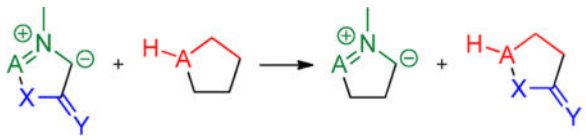

(3)

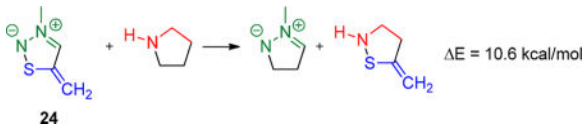

(4)

does not attempt to measure an actual “aromatic stabilization energy” but instead focuses on the “resonance stabilization energy” (RSE) of the 1,3-dipole moieties, induced by delocalization into the adjacent X and C═Y groups. Unsurprisingly, eq 3 predicts that isolating the dipole from the X and Y substituents is disfavored, with each substitution pattern affording a different degree of stabilization for AY and AI (Table 2). The relevance of these differences of stabilization energies will be demonstrated below.

Transition-State Geometries and Energies

The M06-2X/6-31G-(d)-optimized transition structures for the cycloadditions of azomethine ylides **1–12** and azomethine imines **13–24** with acetylene are shown in Figure 5, along with their corresponding activation free energies ($\Delta G^{\ddagger}$) and reaction free energies (ΔG_{rxn}). The TSs with ethylene (**1b–24b**) can be found in Figure S6. They are almost identical to those with acetylene; the forming bond lengths to the same termini of the dipoles never differ by more than 0.06 Å and are different by 0.02 Å on average between acetylene and ethylene reactions. Although transition structures with ethylene are not shown in the main text, their energies will be discussed throughout the paper.

Free energies of activation ($\Delta G^{\ddagger}$) for the cycloadditions of azomethine ylides (AY) **1–12** with acetylene are between 13.0 and 24.7 kcal/mol and from 11.8 to 23.4 kcal/mol with ethylene. For azomethine imines (AI) **13–24**, the $\Delta G^{\ddagger}$ are between 23.9 and 36.6 kcal/mol with acetylene and from 22.9 to 35.1 kcal/mol with ethylene. AY transition structures have longer forming bonds than their AI counterparts, indicative of earlier TSs. This is in agreement with their lower activation barriers and greater reaction exothermicities, as predicted by the Hammond postulate.[26] AY transition structures are more asynchronous respective to AI TSs, with the average difference between forming bond distances being 0.12 Å for AY versus 0.05 Å for AI. For most dipoles, switching from endocyclic O to NH or S mainly shortens the bond forming with C(4) (see **1** vs **5** or **9, 13** vs **17** or **21**), which is furthest from the site of the substitution.

The activation free energies of the 48 computed reactions are represented graphically in Figure 6. Four trends can be identified from this graph: (1) Azomethine ylides have activation barriers significantly lower than those of corresponding imines (light colors vs dark colors, two first bins vs two last, for each X and Y combination). Indeed, switching from ylide to imine (e.g., **1** vs **13, 2** vs **14**, etc.) costs 10.6 kcal/mol on average. (2) Reaction of any dipole with ethylene has a lower activation barrier than that with acetylene, on average by 1.1 kcal/mol (gray or black vs light blue or blue bins). (3) Substitution at the endocyclic (X) position raises the cycloaddition activation barriers in the order of O < S < NH for AY and in the order O < NH < S for AI. Over the whole range of combinations,

oxygen at this position is favored on average by 3.2 kcal/mol versus sulfur and by 4.3 kcal/mol versus NH. (4) For a given endocyclic substituent, exocyclic substitution has a great impact barriers. The cycloaddition reactions become more difficult going from exocyclic CH_2, to NH, to O, to S, in steps of about 2.6 kcal/mol.

Kinetic–Thermodynamic Relationship

To explain the trends in the data, we analyzed various relationships between properties of the systems. Figure 7 is a plot of activation energy ($\Delta E^{\ddagger}$) versus reaction energy (ΔE_{rxn}) for cycloadditions of **1–24** with both dipolarophiles. Excellent linear correlations are observed when acetylene and ethylene reactions are analyzed independently (R^2 = 0.93 and 0.96).[27] If all data points are considered together, a lower R^2 value of 0.86 is obtained. Such a correlation is in accord with the Bell–Marcus–Hammond–Evans–Polanyi–Thornton–Leffler relationship.[28] Such linear relationships were previously observed in some computational studies of cycloadditions of tetrazine and other aromatic nitrogen-containing heterocycles,[29] 5-substituted cyclopentadienes,[30] and 3-substituted cyclopropenes,[31] but it is not a general phenomenon for cycloadditions. Indeed, a majority of our investigations about Diels–Alder reactions[32] or 1,3-dipolar cycloadditions[33] have shown barriers that are dependent on distortion energy, not reaction energy.

Relationship between Activation Energy and Resonance Stabilization of the Dipoles

A kinetic–thermodynamic relationship indicates that ground-state stabilization of the dipoles is responsible for the varying activation energies. Figure 8 shows the plot of activation energies with acetylene versus resonance stabilization energy, calculated using eq 3. Very good linear correlations are observed within each dipole type, with slopes being very similar to those of Figure 7 for $\Delta E^{\ddagger}$ versus ΔE_{rxn}. These correlations confirm that the endo- and exocyclic substituent effects on reactivity of mesoionic dipoles can be explained by the difference in resonance stabilization afforded by these substituents. As both dipole types benefit from similar stabilization for given X and Y substituents (Table 2), the reactivity difference between azomethine ylides and imines must have an alternative origin.

Endocyclic atoms (X) bear a lone pair, which can be shared in the heterocyclic ring, giving it a more “aromatic” character. The calculated trend of stability, NH ≅ S > O, reflects the well-known trend of aromaticity in five-membered nitrogen-containing heterocycles, imidazole ≅ thiazole > oxazole.[24] Exocyclic substituents (Y) have a similar effect. Those that best stabilize a negative charge on the Y atom also stabilize the “aromatic” resonance form (**III**) of the mesoionic compound, making it less reactive. The calculated order of stabilization, CH_2 < NH < O < S is the same as the stability of the allyl, enamide, enolate, and thioenolate anions (Figure S5). Thus, to obtain the most reactive dipoles, the most electronegative atoms are favored at the endocyclic position, whereas the least polarizable atoms are best used at the exocyclic position. These trends of mesoionic dipole stabilities are consistent with reported studies of their thermal isomerizations.[34]

Distortion Interaction Analysis

Although the reactivity pattern can be understood qualitatively in terms of reaction energetics, we wished to analyze directly the factors that influence the transition-state

energies. Figure 9 represents a simplified potential energy surface along some reaction coordinate and defines the distortion/interaction model (also called the activation/strain model).[33, 35] In this model, the activation energy of the reaction $\Delta E^{\ddagger}_{act}$ is decomposed into the distortion energy $\Delta E^{\ddagger}_{dist}$ required to distort the reactants to their geometry at the TS and the interaction energy $\Delta E^{\ddagger}_{int}$ between these distorted reactants. Both reactants contribute to the distortion energy, which in our case is composed of the dipole distortion energy $\Delta E^{\ddagger}_{dist\_4\pi}$ and the dipolarophile distortion energy $\Delta E^{\ddagger}_{dist\_2\pi}$.

We computed $\Delta E^{\ddagger}_{int}$, $\Delta E^{\ddagger}_{dist}$, $\Delta E^{\ddagger}_{dist\_4\pi}$, and $\Delta E^{\ddagger}_{dist\_2\pi}$ for the 48 reactions of dipoles **1–24** with acetylene and ethylene. The data can be found in Table S5 and are plotted against the corresponding activation energies $\Delta E^{\ddagger}_{act}$ of these cycloadditions in Figure 10.[36] Interaction energies (black squares) have a very narrow range of values, from −11.1 to −17.2 kcal/mol, and as such do not correlate with the activation energies. The total distortion energy $\Delta E^{\ddagger}_{dist}$ (green triangles) is an excellent predictor of reactivity, as it correlates very well with activation energies. The dipole distortion contribution $\Delta E^{\ddagger}_{dist\_4\pi}$ (purple diamonds) accounts for 66 ± 5% of the total distortion energy and thus also correlates well with activation energies. This is reasonable and can be explained by the fact that planar dipoles with more resonance stabilization are likely to be more costly to distort in the envelope geometry of the TSs, resulting in higher activation barriers.

In reactions with ethylene as dipolarophile, the distortion energy of the 2π component $\Delta E^{\ddagger}_{dist\_2\pi}$ (blue circles) is 3.3 ± 0.4 kcal/mol lower than that for the corresponding reactions with acetylene. This distortion energy difference therefore explains the reactivity difference that we noted between these two dipolarophiles, especially as they engage in TSs of almost identical forming bond distances and thus similar positions of the transition state along the reaction coordinate.

Distortion Interaction along the Reaction Coordinate

For a given X and Y substituent pattern, AI are much less reactive than AY. Moreover, although both dipole types benefit from almost identical RSE when X and Y are constant (Table 2), the distortion energies of each dipole at the TS are very different, as they correlate well with their respective activation energies. Therefore, distortion energy alone might not be enough to accurately describe the reactivity difference between ylides and imines.

To clarify this reactivity difference, we undertook a distortion/interaction analysis along the reaction coordinate. Such analyses were pioneered by the group of Bickelhaupt,[35, 37] and plot the distortion ΔE_{dist}, interaction ΔE_{int}, and total energies ΔE versus the reaction coordinate (RC), identified by some critical parameter. This parameter is usually a forming bond distance important to the reaction studied. However, because initial bond distances for a bimolecular reaction cannot be accurately known if no reactant complex can be located, this choice of parameter does not allow a precise quantification of the reaction progress. We analyzed the reactions of münchnone **1** and sydnone **13** with acetylene, for which the major structural change happening is the puckering of the 3-nitrogen out of the plane of the initially planar five-membered ring of the dipoles (Scheme 1). This puckering is quantifiable and has identical starting and ending values for **1** and **13**, allowing for direct comparison of energies along the RC. Specifically, we defined the RC as the sum of absolute values of

dihedral angles C(5)–O(1)–C(2)–N(3) and O(1)–C(5)–C(4)–N(3), and the results we obtained are plotted in Figure 11. The position of the TS geometries is highlighted by a thin line.

Along the reaction coordinate, distortion of AY **1** is marginally higher than that of AI **13**, which is consistent with **1** having a marginally greater RSE than **13**. The main difference lies in the interaction energy, where at any point of the reaction **1** has much stronger interactions with acetylene. As the TS lies at the point where the slope of distortion is the opposite of the slope of interaction, stronger interactions lead to an *earlier* TS, which will consequently lead to a lower total distortion energy. Therefore, the strength of the orbital interactions explains the difference in reactivity between azomethine ylides and imines.

This conclusion is consistent with previous work of our group,[29, 32d] such as the π orbital on nitrogen termini of dipoles/dienes is more contracted and less available than the one on carbon termini, resulting in less efficient overlap with those of dipolarophiles/dienophiles. Indeed, the HOMO of ylide **1** (−7.78 eV) is higher in energy than that of imine **13** (−8.95 eV), and this causes the primary orbital interactions to be much more beneficial with the ylide. Over the 24 dipoles studied, the ylides all have a higher-energy HOMO than the corresponding imines with identical X and Y substituents (Table S8). However, the orbital energies of the dipoles have poor correlation with activation energies of their reactions with acetylene or ethylene and no correlation whatsoever with their resonance stabilization energies (Figures S10 and S11).

Our distortion/interaction analysis along the reaction coordinate highlights two important effects. First, single-point analysis of vastly different transition states gives results that are unreliable as of the origin of reactivity difference, as was already discussed in length by Bickelhaupt.[37] Second, for D/I along the RC, the choice of reaction coordinate is of utmost importance, and parameters that are quantifiable along the full reaction coordinate and are of similar value at the TS of the reactions studied are beneficial. Even considering these effects, it is important to mention that asynchronous cycloaddition TSs are difficult to properly represent using any single RC, no matter if it is an average or sum of bond lengths or puckering angles.

CONCLUSION

We have studied the structures, stabilities, and 1,3-dipolar cycloaddition reactivities of mesoionic azomethine ylides and imines bearing various endo- and exocyclic heteroatoms. Reactions with ethylene are more facile than acetylene, due to the lower cost of distortion of ethylene. Azomethine ylides are more reactive than azomethine imines because they have higher HOMO energies and exhibit better orbital interactions with the dipolarophiles along the reaction coordinate. Finally, within one type of mesoionic dipole, substitutions at the endo- or exocyclic positions change the resonance stabilization of the 1,3-dipole, and dipoles that are less stabilized are consequently more reactive. This accounts for the correlation observed between kinetics and thermodynamics, as well as the relationship between RSE and distortion energy of the dipoles. Calculating the RSE of mesoionic dipoles is straightforward and provides a way to rationalize experimental results and also to predict the

reactivity of yet-unknown compounds. Considering our computations, mesoionic dipoles bearing exocyclic nitrogens or carbons could be interesting targets for synthesis because they are predicted to have greater cycloaddition reactivity than the parent münchnones or sydnones.

Supplementary Material

Refer to Web version on PubMed Central for supplementary material.

Acknowledgments

P.A.C. gratefully acknowledges the Fonds de recherche du Québec, Nature et Technologies (FRQNT) for a postdoctoral fellowship. We are grateful to the NIH (R01GM109078 to K.N.H.) for financial support of this research. Computations were performed on the Hoffman2 cluster at UCLA and the Extreme Science and Engineering Discovery Environment (XSEDE), which is supported by the NSF (OCI-1053575). We thank Brian Levandowski and Jason Fell for helpful discussions.

References

1. (a) Potts, KT. Mesoionic Ring Systems. In: Padwa, A., editor. 1,3-Dipolar Cycloaddition Chemistry. Vol. 2. Wiley; New York: 1984. p. 1-82.(b) Gribble, GW. Mesoionic Ring Systems. In: Padwa, A., Pearson, WH., editors. The Chemistry of Heterocyclic Compounds: Synthetic Applications of 1,3-Dipolar Cycloaddition Chemistry Toward Heterocycles and Natural Products. Vol. 59. John Wiley & Sons; Hoboken, NJ: 2002. p. 681-753.(c) Gingrich, HL., Baum, JL. Chemistry of Heterocyclic Compounds: Oxazoles. Vol. 45. Wiley; New York: 1986. Mesoionic Oxazoles; p. 731-961.(d) Gribble, GW. Oxazoles: Synthesis, Reactions, and Spectroscopy, Part A. Vol. 60. Wiley; Hoboken, NJ: 2003. Mesoionic Oxazoles; p. 473-576.
2. Ollis WD, Ramsden CA. Adv. Heterocycl. Chem. 1976; 19:1–122.
3. (a) Huisgen R, Gotthardt H, Bayer HO. Angew. Chem., Int. Ed. Engl. 1964; 3:135–136.(b) Huisgen R, Gotthardt H, Bayer HO, Schaefer FC. Angew. Chem., Int. Ed. Engl. 1964; 3:136–137.
4. For a recent review, see: Reissig H-U, Zimmer R. Angew. Chem., Int. Ed. 2014; 53:9708–9710.
5. (a) Earl JC, Mackney AW. J. Chem. Soc. 1935:899–900.(b) Eade RA, Earl JC. J. Chem. Soc. 1946:591–593. [PubMed: 20282426]
6. For a recent review, see: Browne DL, Harrity JPA. Tetrahedron. 2010; 66:553–568.
7. For recent examples, see: Lopchuk JM, Gribble GW. Tetrahedron Lett. 2015; 56:3208–3211.Sugimoto K, Miyakawa Y, Tokuyama H. Tetrahedron. 2015; 71:3619–3624.
8. For recent examples, see: Erguven H, Leitch DC, Keyzer EN, Arndtsen BA. Angew. Chem., Int. Ed. 2017; 56:6078–6082.Brown AW, Comas-Barceló J, Harrity JPA. Chem. - Eur. J. 2017; 23:5228–5231. [PubMed: 28263411] Decuypere E, Specklin S, Gabillet S, Audisio D, Liu H, Plougastel L, Kolodych S, Taran F. Org. Lett. 2015; 17:362–365. [PubMed: 25545588] Lopchuk JM, Gribble GW. Tetrahedron Lett. 2014; 55:2809–2812.Foster RS, Jakobi H, Harrity JPA. Org. Lett. 2012; 14:4858–4861. [PubMed: 22934538] Lopchuk JM, Gribble GW. Tetrahedron Lett. 2011; 52:4106–4108.Lopchuk JM, Gribble GW. Heterocycles. 2011; 82:1617–1631.Fang Y, Wu C, Larock RC, Shi F. J. Org. Chem. 2011; 76:8840–8851. [PubMed: 21970468]
9. For recent examples, see: Handa NV, Li S, Gerbec JA, Sumitani N, Hawker CJ, Klinger D. J. Am. Chem. Soc. 2016; 138:6400–6403. [PubMed: 27180658] Leitch DC, Kayser LV, Han ZY, Siamaki AR, Keyzer EN, Gefen A, Arndtsen BA. Nat. Commun. 2015; 6:7411. [PubMed: 26077769] Marco-Martínez J, Reboredo S, Izquierdo M, Marcos V, López JL, Filippone S, Martín N. J. Am. Chem. Soc. 2014; 136:2897–2904. [PubMed: 24483247]
10. (a) Narayanam MK, Liang Y, Houk KN, Murphy JM. Chem. Sci. 2016; 7:1257–1261.(b) Wallace S, Chin JW. Chem. Sci. 2014; 5:1742–1744. [PubMed: 25580211] (c) Kolodych S, Rasolofonjatovo E, Chaumontet M, Nevers M-C, Créminon C, Taran F. Angew. Chem., Int. Ed. 2013; 52:12056–12060.
11. See the Supporting Information for details.

12. This retro-cycloaddition step is likely to be spontaneous with alkynes but depends on the dipolarophile (alkyne or alkene), its substituents, and the nature of X═C═Y. These effects might be studied in the future.
13. (a) Huisgen R, Funke E, Schaefer FC, Gotthardt H, Brunn E. Tetrahedron Lett. 1967; 8:1809–1814. (b) Funke E, Huisgen R, Schaefer FC. Chem. Ber. 1971; 104:1550–1561.
14. Potts KT, Husain S. J. Org. Chem. 1970; 35:3451–3456.
15. Masuda K, Adachi J, Nomura K. J. Chem. Soc., Perkin Trans. 1. 1979:956–959.
16. Frisch, MJ., et al. Gaussian 09, revision D.01. Gaussian, Inc.; Wallingford, CT: 2013.
17. Zhao Y, Truhlar DG. Theor. Chem. Acc. 2008; 120:215–241.
18. Lan Y, Zou L, Cao Y, Houk KN. J. Phys. Chem. A. 2011; 115:13906–13920. [PubMed: 21967148]
19. (a) Ribeiro RF, Marenich AV, Cramer CJ, Truhlar DG. J. Phys. Chem. B. 2011; 115:14556–14562. [PubMed: 21875126] (b) Zhao Y, Truhlar DG. Phys. Chem. Chem. Phys. 2008; 10:2813–2818. [PubMed: 18464998]
20. Legault, CY. CYLview, 1.0b. Université de Sherbrooke; 2009. (http://www.cylview.org)
21. Simas AM, Miller J, de Athayade Filho PF. Can. J. Chem. 1998; 76:869–872.
22. Katritzky AR, Jug K, Oniciu DC. Chem. Rev. 2001; 101:1421–1450. [PubMed: 11710227]
23. (a) Anjos IC, Vasconcellos MLAA, Rocha GB. Theor. Chem. Acc. 2012; 131:1294.(b) Anjos IC, Rocha GB. J. Comput. Chem. 2015; 36:1907–1918. [PubMed: 26227084] (c) Oziminski WP, Ramsden CA. Tetrahedron. 2015; 71:7191–7198.
24. Cyrañski MK, Krygowski TM, Katritzky AR, Schleyer PvR. J. Org. Chem. 2002; 67:1333–1338. [PubMed: 11846683]
25. Ramsden CA, Oziminski WP. Tetrahedron. 2014; 70:7158–7165.
26. Hammond GS. J. Am. Chem. Soc. 1955; 77:334–338.
27. Identical correlations are obtained when free energies are compared instead. See Figure S7.
28. Jencks WP. Chem. Rev. 1985; 85:511–527.
29. Yang Y-F, Liang Y, Liu F, Houk KN. J. Am. Chem. Soc. 2016; 138:1660–1667. [PubMed: 26804318]
30. Levandowski BJ, Zou L, Houk KN. J. Comput. Chem. 2016; 37:117–123. [PubMed: 26444427]
31. Levandowski BJ, Houk KN. J. Am. Chem. Soc. 2016; 138:16731–16736. [PubMed: 27977194]
32. (a) Paton RS, Kim S, Ross AG, Danishefsky SJ, Houk KN. Angew. Chem., Int. Ed. 2011; 50:10366–10368.(b) Liu F, Paton RS, Kim S, Liang Y, Houk KN. J. Am. Chem. Soc. 2013; 135:15642–15649. [PubMed: 24044412] (c) Levandowski BJ, Houk KN. J. Org. Chem. 2015; 80:3530–3537. [PubMed: 25741891] (d) Fell JS, Martin BM, Houk KN. J. Org. Chem. 2017; 82:1912–1919. [PubMed: 28150495]
33. (a) Ess DH, Houk KN. J. Am. Chem. Soc. 2007; 129:10646–10647. [PubMed: 17685614] (b) Ess DH, Houk KN. J. Am. Chem. Soc. 2008; 130:10187–10198. [PubMed: 18613669] (c) Schoenebeck F, Ess DH, Jones GO, Houk KN. J. Am. Chem. Soc. 2009; 131:8121–8133. [PubMed: 19459632]
34. (a) McCarthy AR, Ollis WD, Ramsden CA. J. Chem. Soc., Perkin Trans. 1. 1974:624–627.(b) Ollis WD, Ramsden CA. J. Chem. Soc., Perkin Trans. 1. 1974:633–638.(c) Ollis WD, Ramsden CA. J. Chem. Soc., Perkin Trans. 1. 1974:638–642.(d) Ollis WD, Ramsden CA. J. Chem. Soc., Perkin Trans. 1. 1974:642–645.(e) Hanley RN, Ollis WD, Ramsden CA. J. Chem. Soc., Perkin Trans. 1. 1979:732–735.(f) Hanley RN, Ollis WD, Ramsden CA. J. Chem. Soc., Perkin Trans. 1. 1979:741–743.
35. Bickelhaupt FM, Houk KN. Angew. Chem., Int. Ed. 2017; 56:10070–10086.
36. Two graphs that plot the reactions with acetylene and ethylene independently can be found in Figures S8 and S9, respectively.
37. (a) Wolters LP, Bickelhaupt FM. WIRES Comput. Mol. Sci. 2015; 5:324–343.(b) Fernández I, Bickelhaupt FM. Chem. Soc. Rev. 2014; 43:4953–4967. [PubMed: 24699791] (c) van Zeist W-J, Bickelhaupt FM. Org. Biomol. Chem. 2010; 8:3118–3127. [PubMed: 20490400]

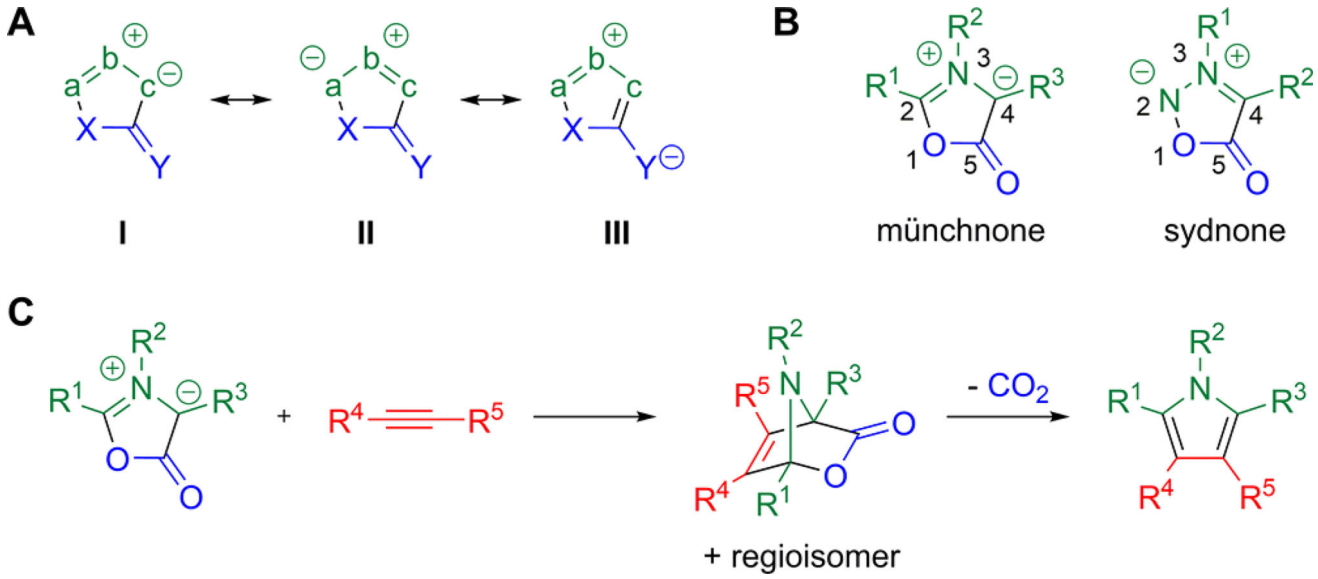

Figure 1.

(A) General structure of a mesoionic ring system, showing three resonance structures. (B) Structure and numbering scheme for common münchnones and sydnones. (C) Reaction pathway for a typical münchnone cycloaddition with an alkyne.

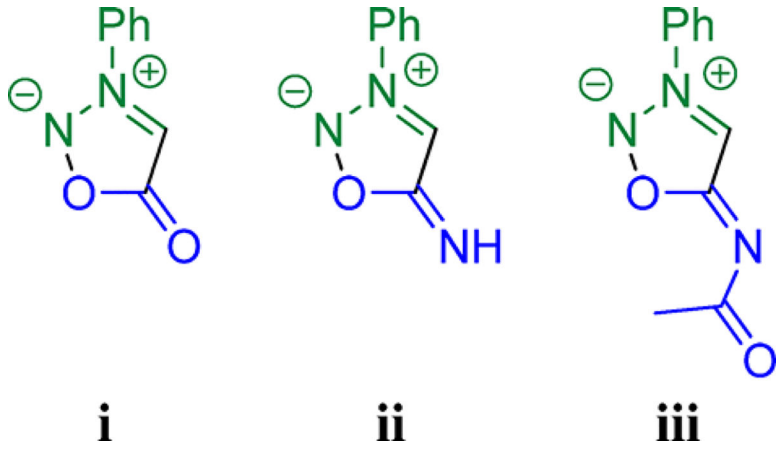

Figure 2.
Mesoionic dipoles investigated for bioorthogonal applications.

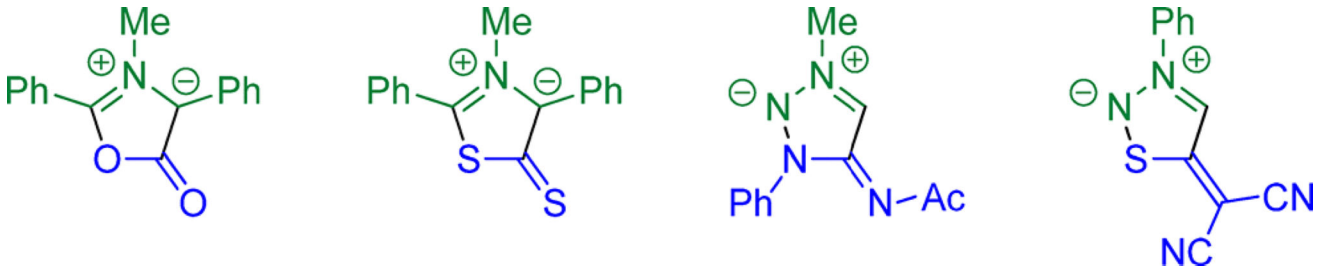

Figure 3.

Examples of reported mesoionic azomethine ylides and imines containing each of the possible endocyclic and exocyclic substituents that are studied here.[3, 13–15]

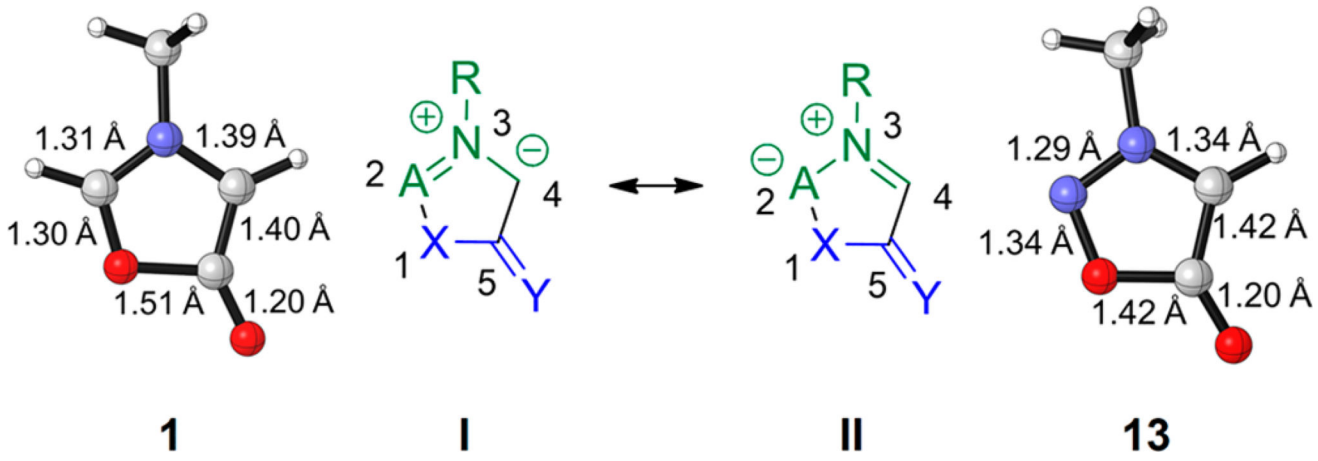

Figure 4.

Structure and key bond lengths (in angstroms) for dipoles **1** and **13** and the resonance structures consistent with these geometries.

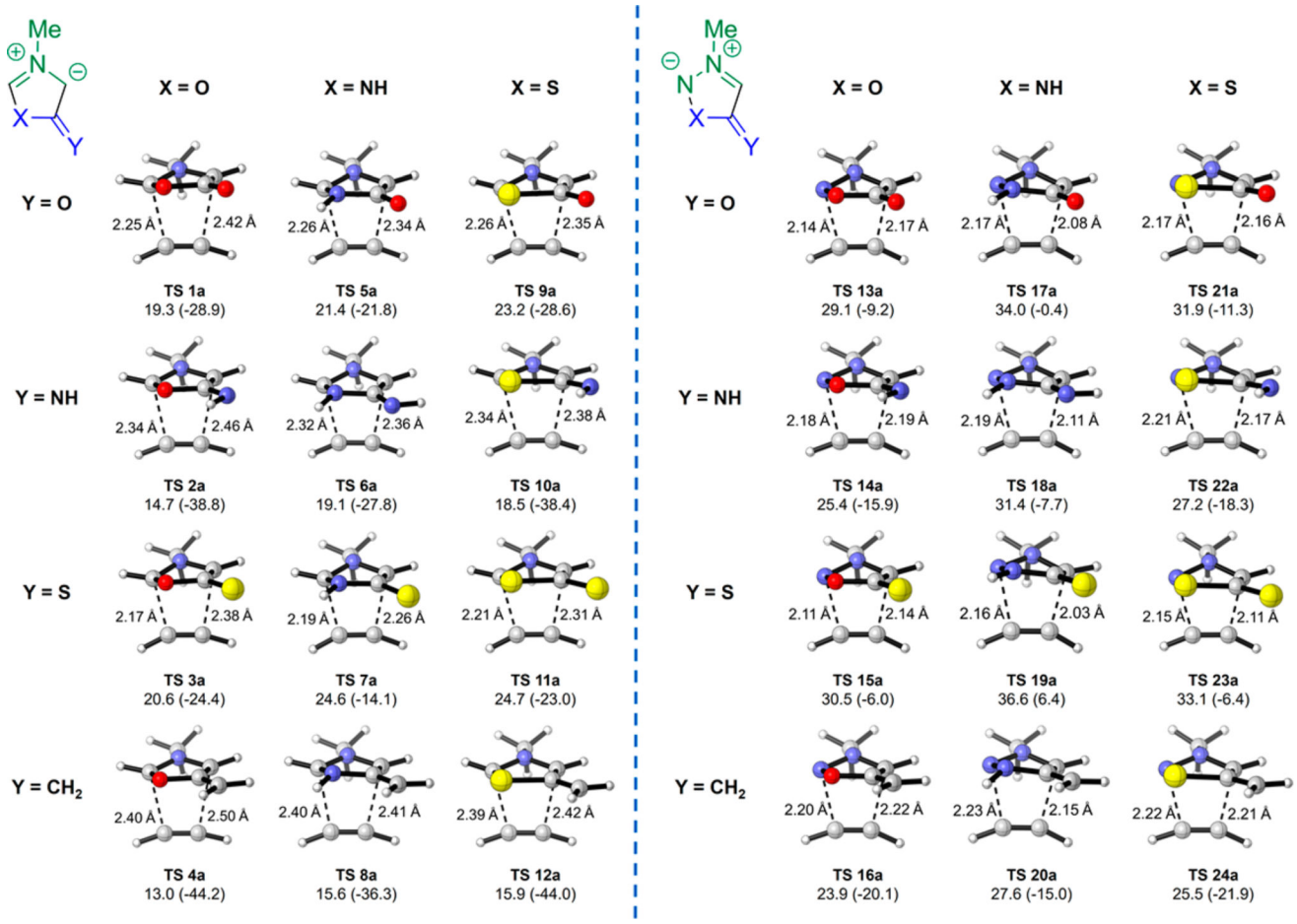

Figure 5.

Optimized transition structures of the 1,3-dipolar cycloaddition of azomethine ylides **1–12** and azomethine imines **13–24** with acetylene and their forming bond distances. $\Delta G^{\ddagger}$ and ΔG_{rxn} (in parentheses) are given in kcal/mol. Structures and free energies of the 24 transition structures with ethylene can be found in Figure S6.

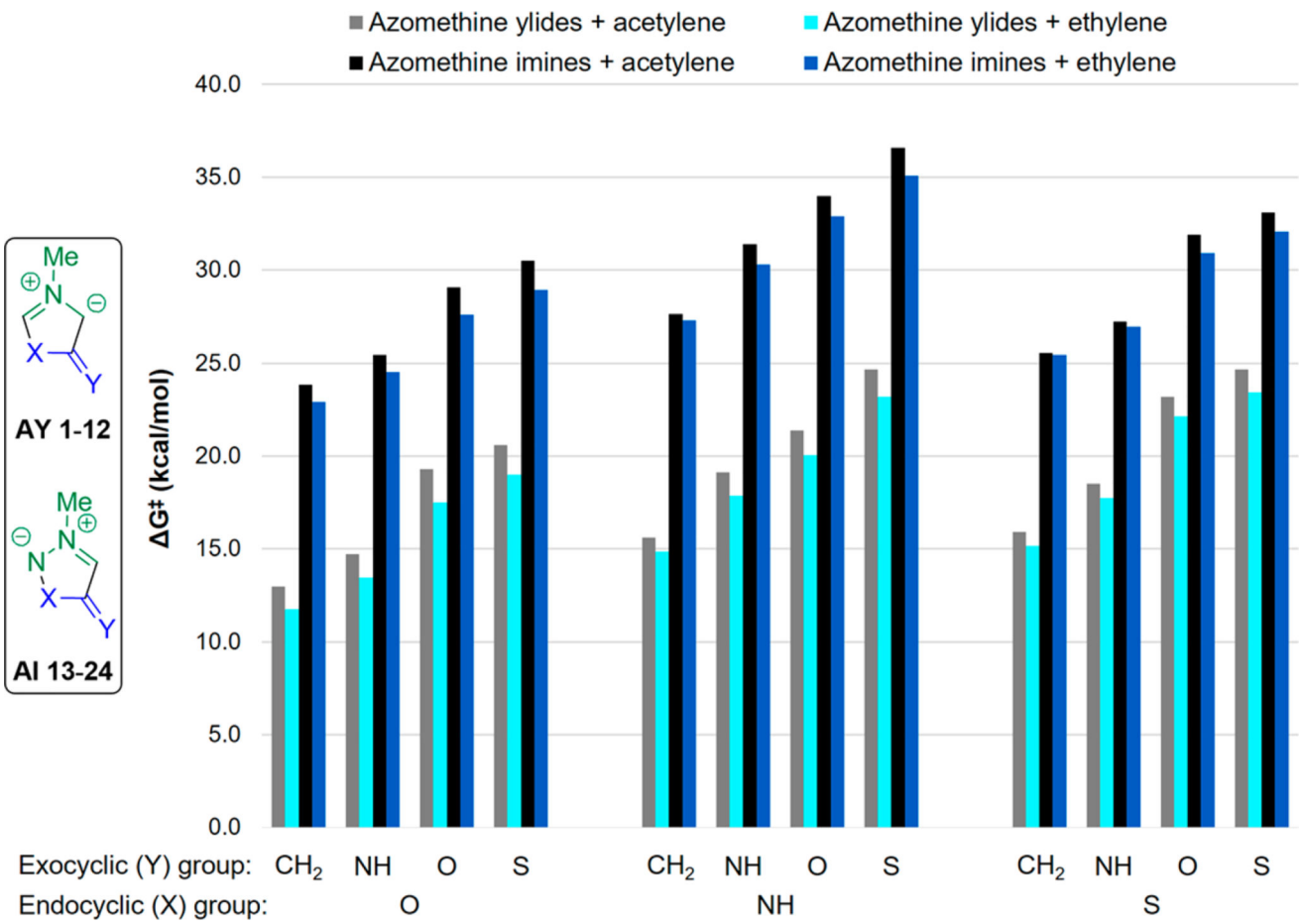

Figure 6.

Activation free energies for the reaction of dipoles **1–24** with acetylene or ethylene. Results are organized by endocyclic and exocyclic substituents of the dipoles. Histogram bars are color-coded to indicate azomethine ylide or imine, reacting with acetylene or ethylene.

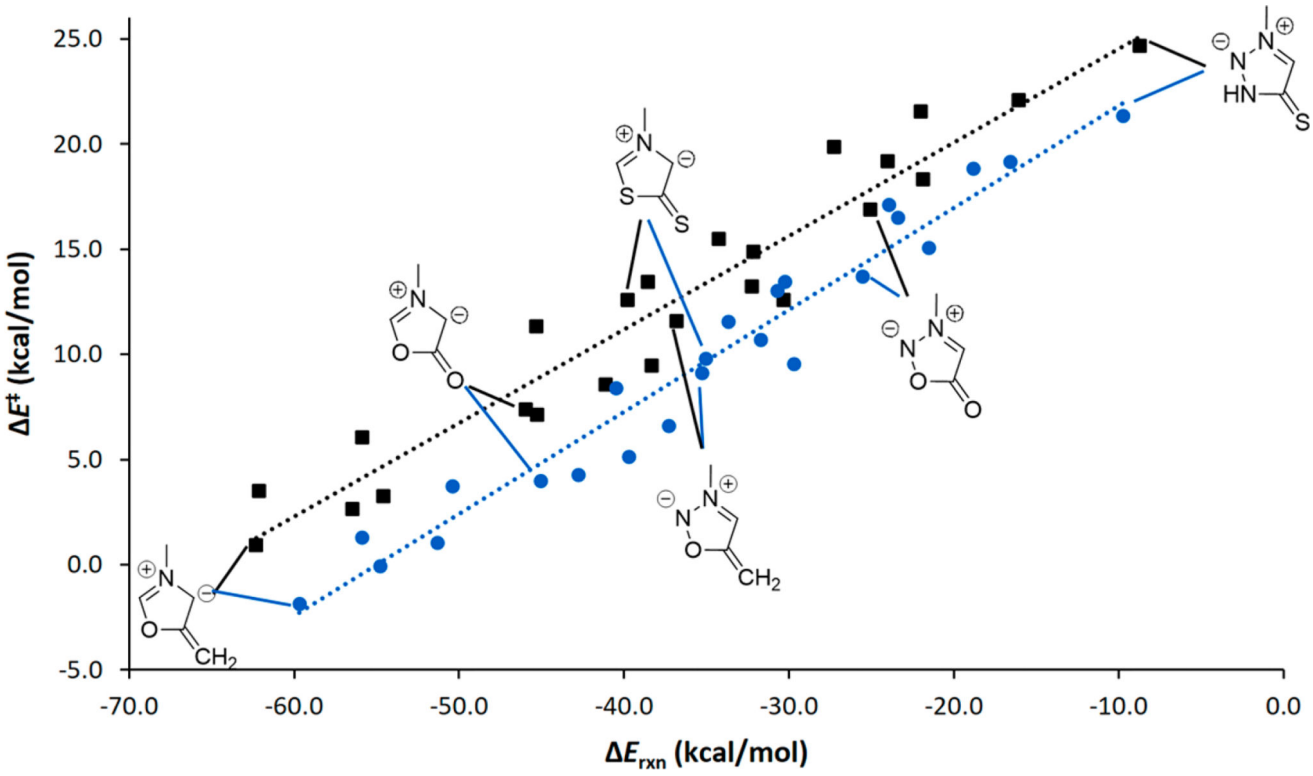

Figure 7.

Plot of activation energy ($\Delta E^{\ddagger}$) versus reaction energy (ΔE_{rxn}) for cycloadditions of **1–24**. Black squares: reaction with acetylene, $\Delta E^{\ddagger} = 0.44\ \Delta E_{rxn} + 29$, $R^2 = 0.93$. Blue circles: reaction with ethylene, $\Delta E^{\ddagger} = 0.49\ \Delta E_{rxn} + 27$, $R^2 = 0.96$. Data points related to some key azomethine ylides and imines are identified for comparison.

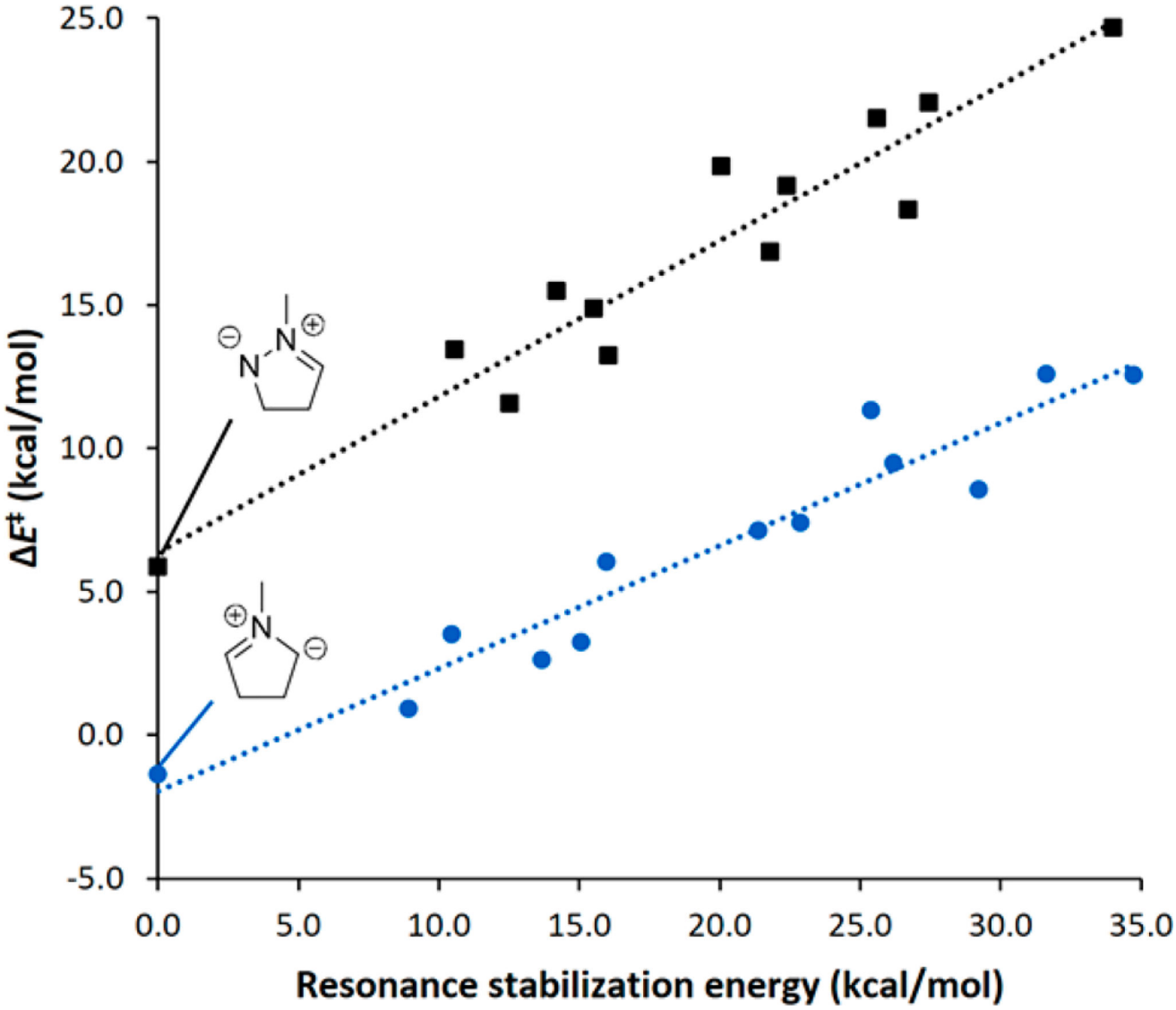

Figure 8.

Plot of activation energy ($\Delta E^{\ddagger}$) for the reaction of dipoles **1–24** with acetylene versus resonance stabilization energy (ΔE_{RSE}) calculated for every dipole. Black squares: azomethine imines, $\Delta E^{\ddagger} = 0.54\ \Delta E_{RSE} + 6.4$, $R^2 = 0.91$. Blue circles: azomethine ylides, $\Delta E^{\ddagger} = 0.43\ \Delta E_{RSE} - 1.9$, $R^2 = 0.93$.

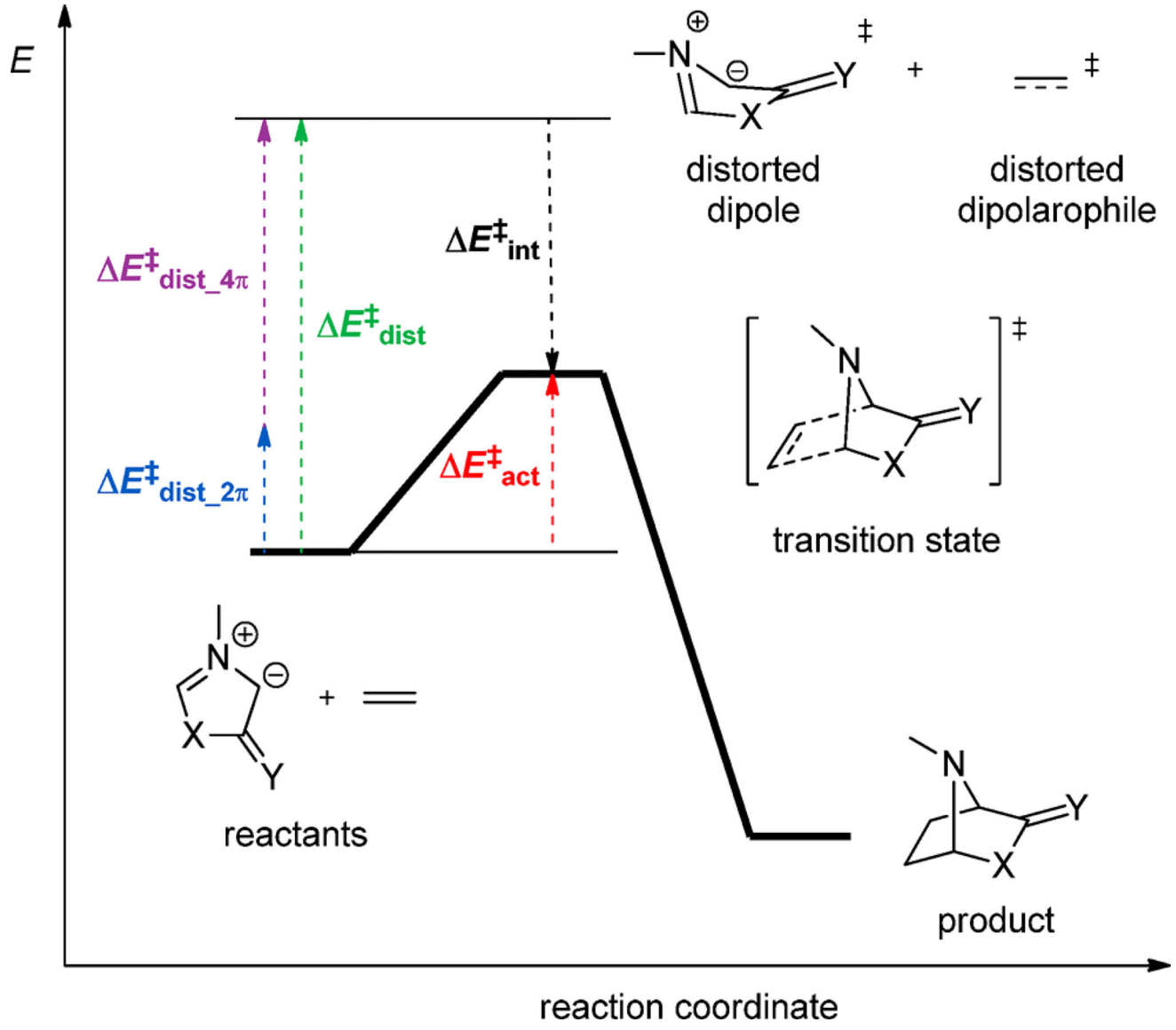

Figure 9.
Distortion/interaction model.

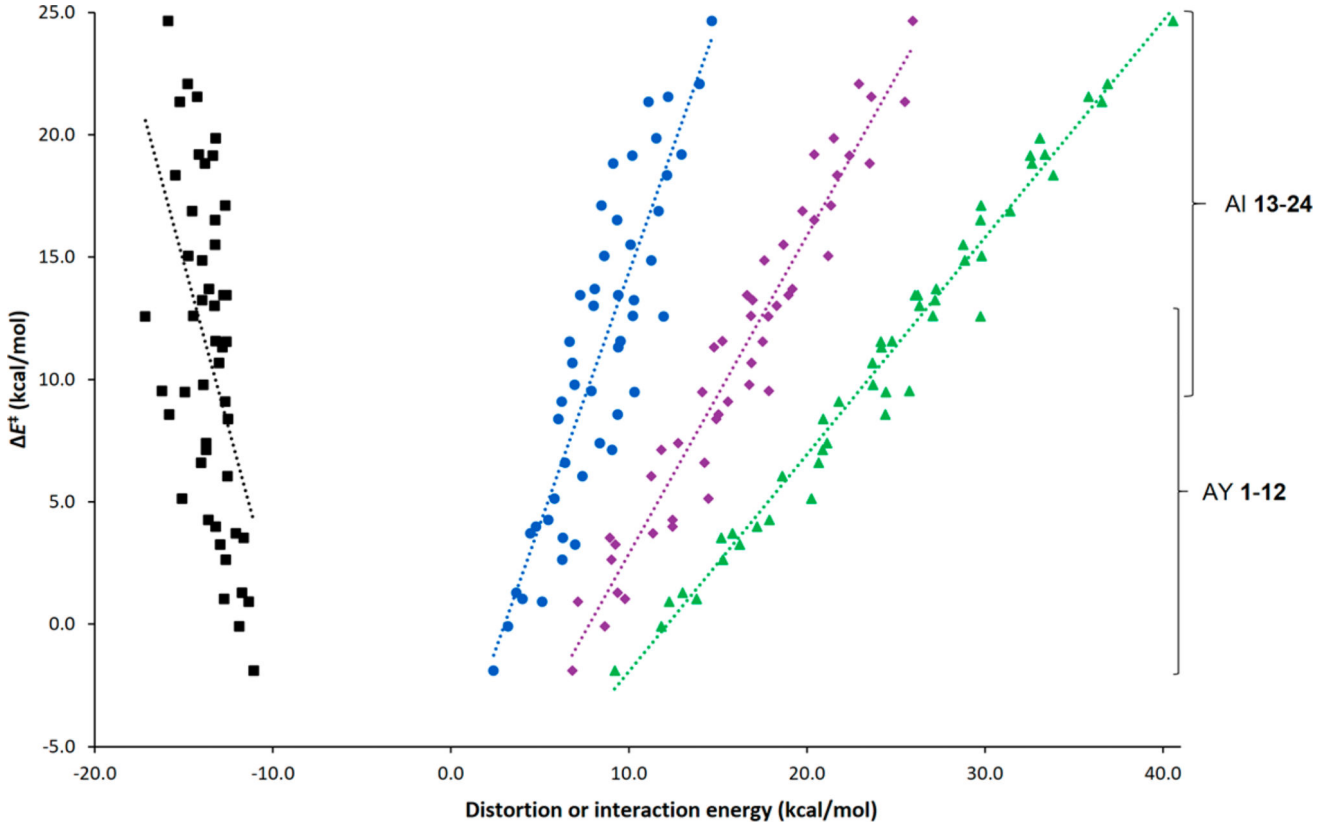

Figure 10.

Plot of activation energy ($\Delta E^{\ddagger}$) versus interaction energy ($\Delta E^{\ddagger}_{int}$, black squares, $\Delta E^{\ddagger} = -2.7\ \Delta E^{\ddagger}_{int} - 26$, $R^2 = 0.28$), dipolarophile distortion energy ($\Delta E^{\ddagger}$, blue circles, $\Delta E^{\ddagger} = 2.1\ \Delta E^{\ddagger} - 6.2$, $R^2 = 0.78$), dipole distortion energy ($\Delta E^{\ddagger}$, purple diamonds, $\Delta E^{\ddagger} = 1.3\ \Delta E^{\ddagger} - 10$, $R^2 = 0.94$), or total distortion energy ($\Delta E^{\ddagger}$, green triangles, $\Delta E^{\ddagger} = 0.89\ \Delta E^{\ddagger} - 11$, $R^2 = 0.98$).

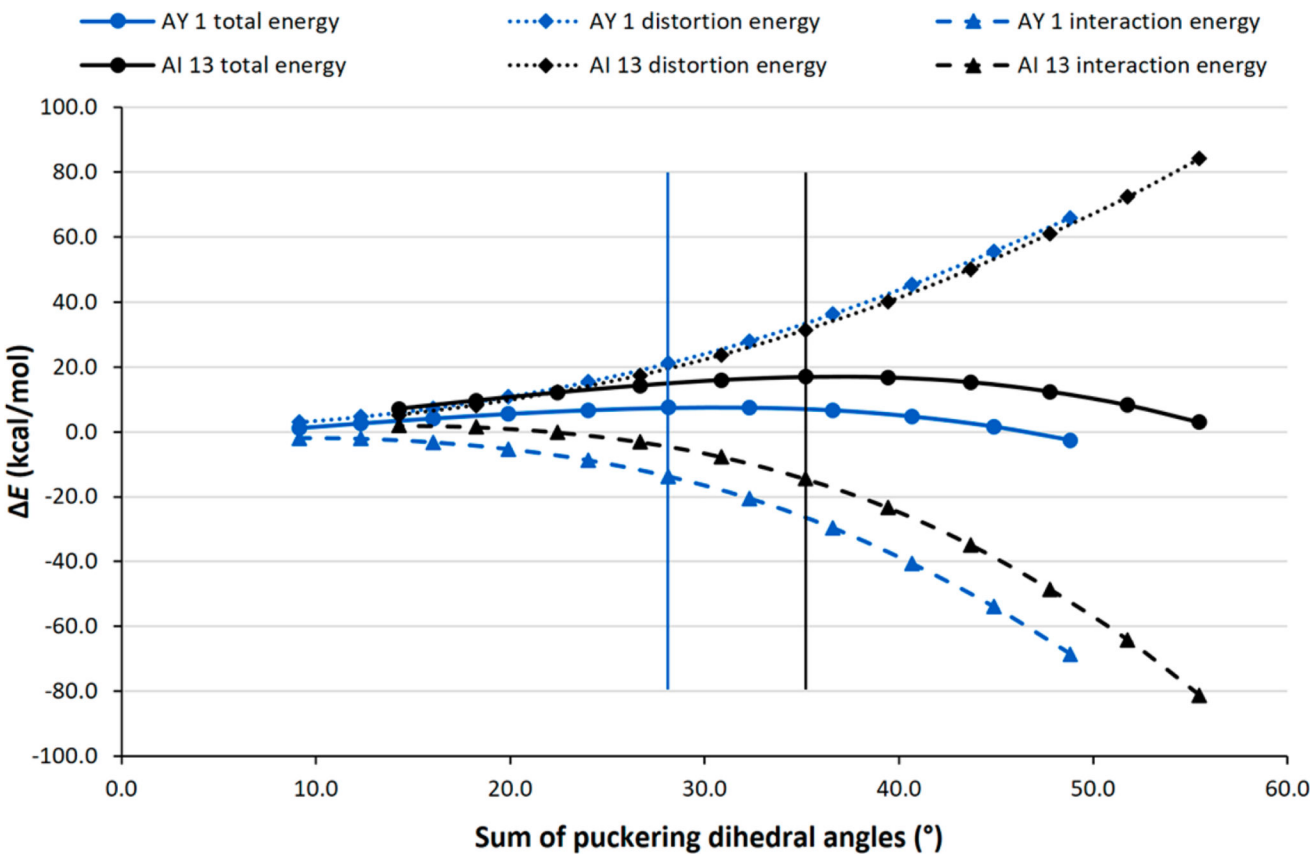

Figure 11.

Distortion/interaction analysis along the reaction coordinate for the reactions of AY **1** (blue) and AI **13** (black) with acetylene.

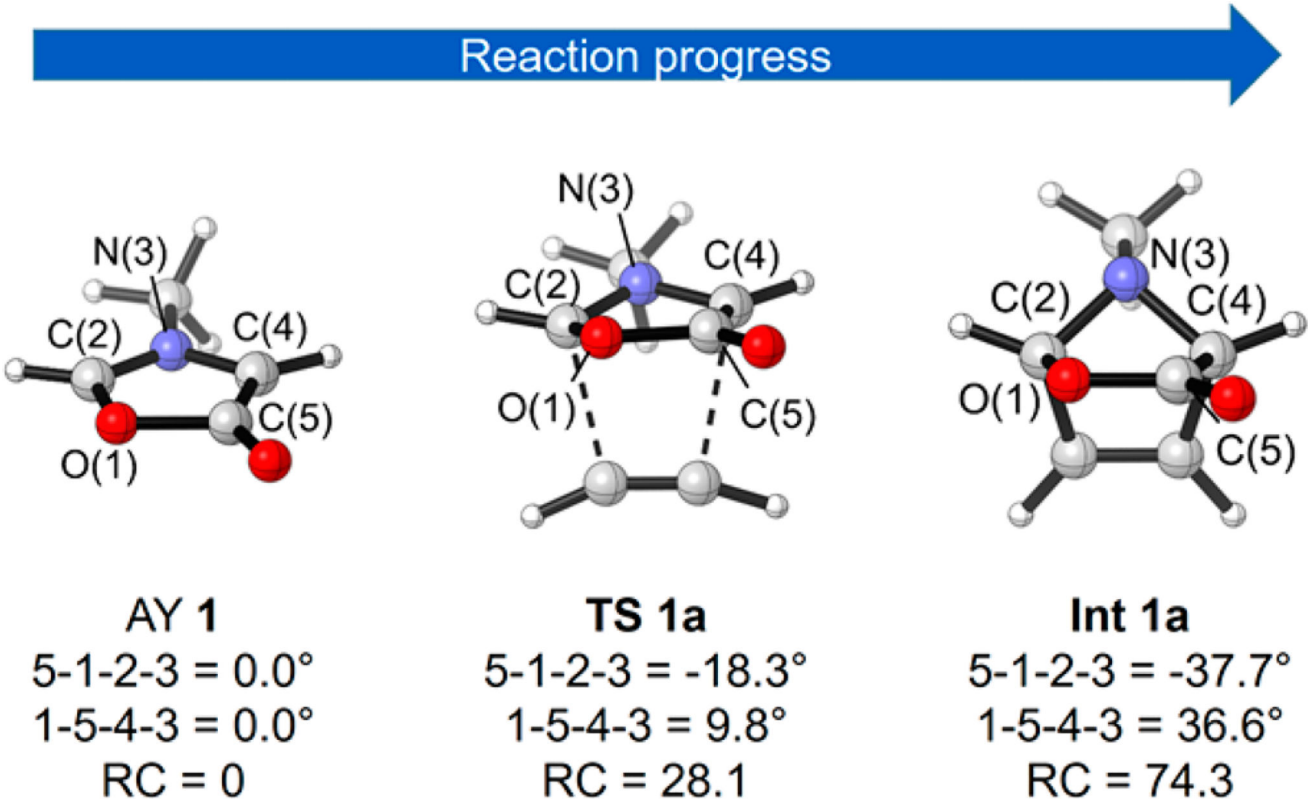

Scheme 1.
Definition of the Reaction Coordinate by the Puckering of the Dihedral Angles in the Dipole

Table 1

1,3-Dipolar Cycloadditions of Azomethine Ylides (A = CH) and Imines (A = N) Studied in the Present Work

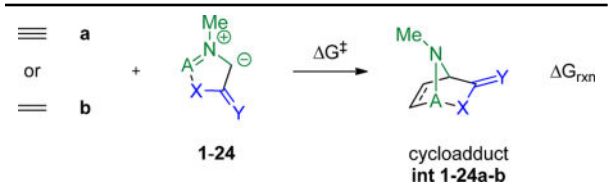

1-24 cycloadduct **int 1-24a-b**

	A = CH			**A = N**		
	X = O	**X = NH**	**X = S**	**X = O**	**X = NH**	**X = S**
Y = O	**1**	**5**	**9**	**13**	**17**	**21**
Y = NH	**2**	**6**	**10**	**14**	**18**	**22**
Y = S	**3**	**7**	**11**	**15**	**19**	**23**
Y = CH_2	**4**	**8**	**12**	**16**	**20**	**24**

J Org Chem. Author manuscript; available in PMC 2017 November 09.

Table 2

Resonance Stabilization Energy (Calculated from eq 3, in kcal/mol) of AY (A = CH) 1–12 and AI (A = N) 13–24, as a Function of Their X and Y Substituents

	A = CH						A = N					
	X = O		X = NH		X = S		X = O		X = NH		X = S	
Y = O	**1**	22.9	**5**	26.2	**9**	25.4	**13**	22.9	**17**	27.4	**21**	20.0
Y = NH	**2**	13.7	**6**	21.4	**10**	16.0	**14**	16.0	**18**	22.4	**22**	14.2
Y = S	**3**	29.2	**7**	34.7	**11**	31.6	**15**	26.7	**19**	34.0	**23**	25.6
Y = CH_2	**4**	8.9	**8**	15.1	**12**	10.5	**16**	12.5	**20**	15.5	**24**	10.6